

Article

Ultra-Broadband Plasmon Resonance in Gold Nanoparticles Precipitated in ZnO-Al₂O₃-SiO₂ Glass

Georgiy Shakhgildyan ^{1,*}, Leon Avakyan ², Grigory Atroshchenko ¹, Maxim Vetchinnikov ¹, Alexandra Zolikova ¹, Elena Ignat'eva ¹, Mariam Ziyatdinova ¹, Elena Subcheva ³, Lusegen Bugaev ² and Vladimir Sigaev ¹

¹ Department of Glass and Glass-Ceramics, Mendeleev University of Chemical Technology, 125047 Moscow, Russia

² Physical Faculty, Southern State University, 344090 Rostov-on-Don, Russia

³ Biomaterials Resource Center, Sirius University of Science and Technology, 354340 Sirius, Russia

* Correspondence: shakhgildian.g.i@muctr.ru

Abstract: Optical materials with a tunable localized surface plasmon resonance (LSPR) are of great interest for applications in photonics and optoelectronics. In the present study, we explored the potential of generating an LSPR band with an ultra-broad range of over 1000 nm in gold nanoparticles (NPs), precipitated through a thermal treatment in ZnO-Al₂O₃-SiO₂ glass. Using optical absorption spectroscopy, we demonstrated that the LSPR band's position and shape can be finely controlled by varying the thermal treatment route. Comprehensive methods including Raman spectroscopy, X-ray diffraction, and high-resolution transmission electron microscopy were used to study the glass structure, while computational approaches were used for the theoretical description of the absorption spectra. The obtained results allowed us to suggest a scenario responsible for an abnormal LSPR band broadening that includes a possible interparticle plasmonic coupling effect taking place during the liquid-liquid phase separation of the heat-treated glass. The formation of gold NPs with an ultra-broad LSPR band in glasses holds promise for sensitizing rare earth ion luminescence for new photonics devices.

Keywords: gold nanoparticles; glass; surface plasmon resonance; LSPR; plasmonics; phase separation; microstructure



Citation: Shakhgildyan, G.; Avakyan, L.; Atroshchenko, G.; Vetchinnikov, M.; Zolikova, A.; Ignat'eva, E.; Ziyatdinova, M.; Subcheva, E.; Bugaev, L.; Sigaev, V. Ultra-Broadband Plasmon Resonance in Gold Nanoparticles Precipitated in ZnO-Al₂O₃-SiO₂ Glass. *Ceramics* **2024**, *7*, 562–578. <https://doi.org/10.3390/ceramics7020037>

Academic Editors: Maurice Gonon, Sandra Abdelouhab and Gisèle Laure Lecomte-Nana

Received: 3 April 2024
Revised: 16 April 2024
Accepted: 17 April 2024
Published: 25 April 2024



Copyright: © 2024 by the authors. Licensee MDPI, Basel, Switzerland. This article is an open access article distributed under the terms and conditions of the Creative Commons Attribution (CC BY) license (<https://creativecommons.org/licenses/by/4.0/>).

1. Introduction

Gold nanoparticles (NPs) have emerged as a central figure in the advancement of nanotechnology and materials science, owing to their unique optical properties, particularly the phenomenon of localized surface plasmon resonance (LSPR) [1]. This phenomenon, which results from the collective oscillation of conduction band electrons in gold NPs under light excitation, has fueled extensive research due to its potential applications across a broad spectrum of fields including photonics, optoelectronics, biomedicine, and sensing technologies [2,3]. The optical properties of gold NPs, such as their absorption and scattering spectra, are governed by LSPR, which can be finely tuned across the visible and near-infrared spectrum by adjusting the NPs' physical parameters. Research has shown that the size of gold NPs plays a critical role in determining their LSPR characteristics, with smaller particles predominantly absorbing light and larger particles scattering it. For instance, it was demonstrated that the LSPR wavelength redshifts as the size of the gold nanosphere increases, highlighting the tunability of NPs for specific applications based on size adjustments alone [4]. Furthermore, the shape of gold NPs significantly impacts their optical properties, with non-spherical nanoparticles such as rods, triangles, and stars exhibiting multiple plasmon resonance peaks corresponding to their various geometrical features. It was shown that the shape and geometry of gold nanorods influence their optical absorption and local field enhancement, crucial for applications in surface-enhanced Raman

spectroscopy [5]. The surrounding dielectric environment also modifies the LSPR of gold NPs, affecting their optical sensitivity and enabling the design of environment-responsive systems. Djorović et al. introduced a method to enhance the characterization of gold NPs through the measurement of the extinction to absorption ratio, offering a new way to assess the volume and dielectric function of NPs with increased accuracy [6].

This tunability of the LSPR, coupled with the strong electromagnetic field enhancement near the nanoparticle surface, makes gold NPs ideal candidates for enhancing the performance of photonic devices, especially in the field of new optical media [7]. The enhancement of rare earth ions (REIs) luminescence through the LSPR of gold NPs presents a sophisticated interplay of multifactorial dependencies critical for the advancement of photonic and optoelectronic devices. This enhancement process is primarily governed by the energy overlap between the LSPR of the gold NPs and the absorption energies of the REIs, which are suitable for their excitation [8]. Hence, the precise tuning of the LSPR band for specific REIs is crucial for the development of advanced optical materials.

One of the most suitable media for the development of optical materials utilizing the advantages of gold NPs and REI interactions is glass. The incorporation of gold NPs into glass matrices provides a promising platform for exploiting the LSPR phenomena, enabling novel applications in optics, sensing, and photonics [9]. Hence, beyond their aesthetic appeal, glasses embedded with gold NPs have garnered significant interest for applications in photonics and nonlinear optics [10,11]. The integration of gold NPs into glasses combines the desirable mechanical and chemical properties of the glass matrix with the unique plasmonic properties of the NPs. This synergy is being explored for the development of efficient laser materials for enhancing the third-order nonlinear optical susceptibility and for surface-enhanced Raman spectroscopy. As in other media, the efficacy of these applications of gold NPs formed in glass is critically dependent on the characteristics of the LSPR band, which in turn are influenced by the abovementioned factors. Recent experiments have demonstrated the formation of gold NPs in glass with a red-shifted LSPR band in different glass systems [12–14]. Laser irradiation of glass also marks a significant leap forward in the domain of the formation of NPs with tunable LSPR bands [15–17]. These studies collectively underline the significant potential of gold NPs in glass matrices for enhancing and manipulating LSPR for various technological applications. But the ability to tune the plasmonic properties of NPs in a wide range remains a challenge, the solution to which can open new opportunities for the development of advanced optical devices and sensors, exploiting the unique interactions between light and matter at the nanoscale.

Hence, in this study, we explored for the first time the potential of gold NPs precipitation in ZnO-Al₂O₃-SiO₂ glass and showed the possibility of generating an ultra-broad LSPR band. The obtained results allowed us to suggest a scenario responsible for such abnormal LSPR band broadening, which included a possible interparticle plasmonic coupling effect taking place during the liquid–liquid phase separation of the glass under the heat treatment. The formation of gold NPs with an ultra-broad LSPR band in glasses holds promise for sensitizing REIs for new photonics devices.

2. Materials and Methods

2.1. Glass Synthesis

In this work, we synthesized glass with the following nominal composition (mol.%): 1.0 SnO₂; 25.0 Al₂O₃; 25.0 ZnO; and 49.0 SiO₂, with 0.01% of AuCl₃, which was introduced in addition to the 100%. The glass batch calculated to produce 500 g of glass was prepared using high-purity raw materials (SiO₂, Al(OH)₃, ZnO, SnO₂, AuCl₃) thoroughly mixed together. The glass was melted at 1590 °C for 6 h in a 600 mL silica crucible in the laboratory electric furnace with SiC heating elements. The glass was casted in the preheated steel mold and subsequently annealed at 600 °C for 4 h in the muffle furnace. The resulted glass casting exhibited high quality, a significant part of which was free of striae and bubbles. The most homogeneous parts of obtained glass were cut into plates and polished. To

study the effect of gold NPs formation, synthesized glass samples were heat-treated in the muffle furnace at various temperatures in the 750–850 °C range for 5 and 20 h. All of the heat-treated samples will be referred to further as “temperature-time” (e.g., 750-20).

2.2. Glass Characterization

The visual appearance of the samples was captured by a digital camera in transmitted and reflected light. For the determination of the glass transition temperature (T_g) and the crystallization temperature (T_C), differential scanning calorimetry (DSC) was used. A bulk glass sample of about 20 mg was heated in a Pt crucible using the simultaneous thermal analyzer STA 449 F3 Jupiter (NETZSCH, Selb, Germany) with a dynamic flow atmosphere of Ar. The temperature range was from room temperature to 1200 °C with a heating rate of 10 °C/min. X-ray diffraction (XRD) patterns of the powdered samples were recorded by means of a diffractometer D2 Phaser (Bruker, Billerica, MA, USA) employing nickel-filtered $\text{CuK}\alpha$ radiation. Raman spectra were collected from the polished glass samples using an NTEGRA Spectra spectrometer, (NT-MDT Co., Moscow, Russia) with an argon (Ar) laser beam (488 nm excitation wavelength). The optical absorption and reflectance spectra of the samples were recorded in the 200–1650 nm spectral range by the spectrophotometer UV-3600 (Shimadzu, Kyoto, Japan). The bulk glass refractive index was determined at 589.3 nm by an DR-M4 Abbe refractometer (ATAGO, Tokyo, Japan).

The microstructure of the samples was studied by a high-resolution transmission electron microscopy (HRTEM) with the transmission electron microscope JEM-2100Plus (JEOL, Peabody, MA, USA) in the 200 kV mode. Bulk glass samples were grounded in an agate mortar to fine powders and dispersed in ethanol. The obtained solution was dropped on a microscope grid, which was dried for 20 min. Images were obtained in the bright field mode on different parts of the grid loaded with the material, providing a fairly complete and objective visualization of the samples. The HRTEM images were analyzed with ImageJ software version 1.53n (direct measurement of particle sizes and interparticle distances (number of measured units exceed 50); and measurement of the lattice spacings of crystal particles on the Fourier-filtered region of the image) [18,19].

3. Results

3.1. Optical Properties of Glasses upon Heat Treatment

The DSC curve of the synthesized glass shows two exothermic peaks corresponding to the crystallization of different phases; the T_g temperature of the glass is 750 °C (Figure S1). The glass composition chosen in this work is close to one of the compositions (namely ZAS50.25) from a recent study that investigated the glass formation and crystallization region in the $\text{ZnO-Al}_2\text{O}_3\text{-SiO}_2$ system [20]. A comparison of the T_g temperatures and number of exothermic peaks shows a general similarity, while some differences in the values of crystallization temperatures (T_C) can be related to the different conditions of glass synthesis in this work and in [20].

The raw glass was transparent without visible signs of crystallization or coloration, and its absorption spectrum also did not show any bands in the visible and near-infrared spectral region (Figure 1). The refractive index n_D of the glass was 1.569. Heat treatment of glass at temperatures above T_g led to a noticeable coloration of the samples, which is expected for glasses containing gold and a small addition of SnO_2 [21]. However, in contrast to the red (ruby) coloring typical for silicate glasses with gold, heat treatment of glasses for 5 h in the range of 800–850 °C led to the appearance of a turquoise color which, with an increase in the treatment temperature, changed to blue (Figure 1, inset). It should be noted that the above colors were observed when the samples were studied in transmitted light; at the same time, when the angle of illumination was changed and the samples were observed in reflected light, the color of the samples changed to brown. The intensity of this effect increases with increasing treatment temperature: for sample 800-5, the effect is weakly pronounced (not distinguishable on the photo), and for sample 850-5 with maximum treatment temperature, the effect is clearly visible. The observed effect

can be attributed to a dichroism phenomenon (color change in transmitted and reflected light). In previous works, the dichroism effect was obtained in glasses of phosphate systems containing both gold and copper NPs [22–24]; in tellurite glasses with gold NPs [14]; and in glasses of the $K_2O-B_2O_3-Sb_2O_3-ZnO$ system, also containing gold NPs [25]. The nature of dichroism in glasses with NPs is complex and has not yet been unequivocally established.

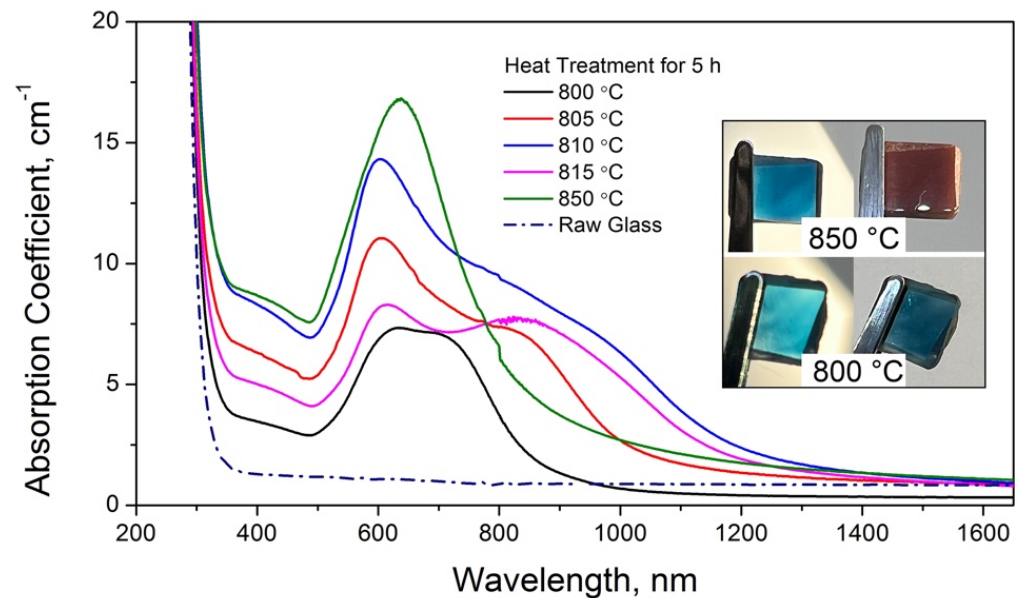


Figure 1. Absorption spectra of the raw glass and glasses heat-treated in the 800–850 °C range for 5 h. Insets show visual appearance of glasses treated at 800 and 850 °C in transmitted and reflected light (left and right panel, respectively). Each glass sample size is $\approx 1 \text{ cm} \times 1 \text{ cm}$.

The absorption spectra of glasses heat-treated for 5 h (Figure 1) show the presence of bands, the shape and intensity of which strongly depend on the treatment temperature. Because the absorption spectra of synthesized glasses of the same composition but without gold and heat-treated under the same regimes show no absorption bands (the spectra are not shown in this work), we attribute the bands in Figure 1 to the LSPR of gold NPs. An analysis of the experimental spectra shows that at the minimum treatment temperature (800 °C), a broad band with an asymmetric plateau extending from ≈ 630 to 750 nm is formed. Increasing the treatment temperature leads to an increase in the intensity of the band and strengthening of asymmetry: a maximum at 603 nm and a broad shoulder with a maximum at ≈ 810 nm are formed.

A further increase in temperature (up to 810 °C) intensifies the short-wave band, the maximum of which shifts to ≈ 610 nm; the long-wave shoulder broadens, and its intensity slightly increases. The increase in treatment temperature to 815 °C leads to the formation of a band with two maxima that are almost equal in intensity (at 613 and 823 nm). A further increase in temperature up to 850 °C leads to the formation of a symmetric band with one maximum at 638 nm. Such a sequence of changes in the LSPR bands of gold NPs in glasses seems atypical and has not been previously described in the literature. To study this phenomenon in more detail, we carried out a series of heat treatments of glass samples at a longer exposure time (20 h).

Figure 2 shows the absorption spectra of glasses after the heat treatment in the range of 750–820 °C for 20 h, as well as the photographs of some samples. Analysis of the appearance of the samples obtained after the temperature treatment shows the following dynamics: Treatment at T_g temperature (750 °C) leads to a weak coloration of the glass sample in a color close to violet, and the effect of dichroism is not manifested. Increased treatment temperature leads to coloring of the glass in a turquoise-blue color, and with

rising temperature, the intensity of coloring increases. The dichroism effect in these samples appears and intensifies with increasing treatment temperature (Inset in Figure 2).

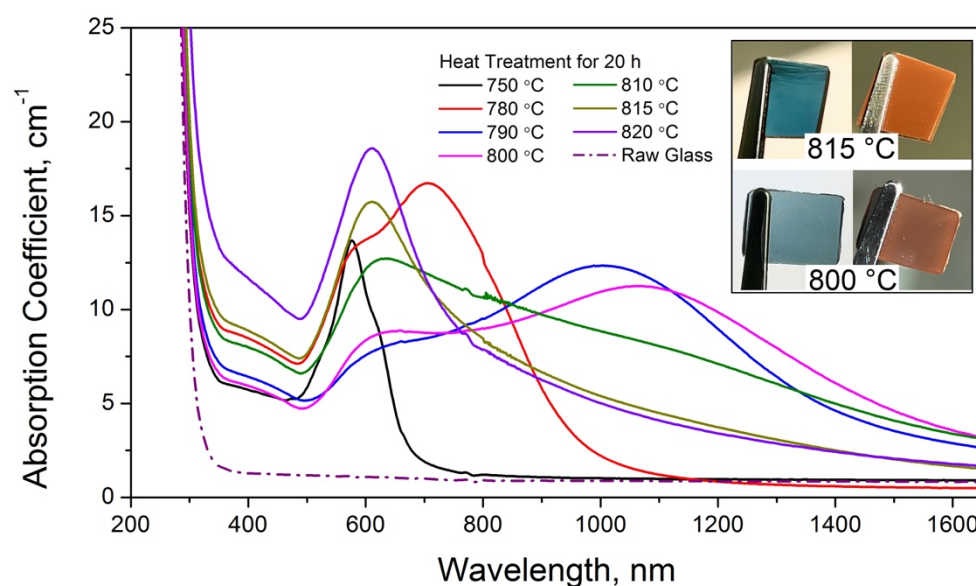


Figure 2. Absorption spectra of the raw glass and glasses heat-treated in the 750–820 °C range for 20 h. Insets show the visual appearance of glasses treated at 800 and 815 °C in transmitted and reflected light (left and right panel, respectively). Each glass sample size is $\approx 1 \text{ cm} \times 1 \text{ cm}$.

Increasing the treatment temperature of the glasses initiates significant changes in the absorption spectra (Figure 2). The LSPR band of sample 750-20 is slightly asymmetric, with a clear maximum at 576 nm and a small long-wavelength shoulder up to 650 nm. For sample 780-20, changes in the band shape are noticeable: the long-wavelength shoulder turns into a broad band with a maximum at 705 nm, and a short-wavelength shoulder at 595 nm also appears. A further increase in the glass treatment temperature up to 800 °C leads to an extraordinary broadening of the LSPR band with the formation of two maxima at 658 and ≈ 1150 nm. At the same time, the long-wavelength shoulder of the band extends beyond 1600 nm. For sample 810-20, there is a sharp change in the shape of the band: there is one maximum at 630 nm, and a broad long-wavelength shoulder is formed, also extending into the IR region. At the maximum treatment temperatures (815 and 820 °C), the band shape becomes similar to sample 850-5 (Figure 1), with the difference being that the band maximum is fixed at 610 nm. To the best of our knowledge, the results obtained for sample 800-20 for the broadening of the LSPR band (more than 1000 nm) are record-breaking.

The pronounced changes in the shape and position of the LSPR band during the heat treatment of glasses in a fairly narrow temperature range indicate significant changes that occur in the structure of glasses. To understand the mechanisms responsible for the changes in the optical properties of glasses, we studied their microstructure.

3.2. Structural Study of Glasses

Figure 3 shows the results of the XRD and Raman spectroscopy analyses of glasses heat-treated for 5 and 20 h. The XRD patterns (Figure 3a,b) show that regardless of the heat treatment conditions, the glasses remain X-ray amorphous, which indicates the absence of crystalline inclusions that can be detected by this method. The absence of the peaks related to Au NPs can be explained by the low concentration of AuCl_3 in the glass composition. Moreover, in [20], in the Au-free glass of similar composition, HT-XRD analysis at 850 °C revealed the presence of a $\text{ZnO-Al}_2\text{O}_3\text{-SiO}_2$ solid solution (ZAS-s.s.) phase (ICDD card #00-032-1455), which was subsequently replaced by a gahnite phase (ICDD card #01-074-1138) at 950 °C. Apparently, in our case, the absence of ZAS-s.s. reflections in the XRD patterns

of the heat-treated glass samples is due to the higher temperature of the first T_{C1} exopeak compared with the above work (992 °C in our case and 907 °C in [20]). However, it can be assumed that at high treatment temperatures in the glasses studied by us, the formation of the ZAS-s.s. phase can begin, the sizes of which are so small that they cannot be detected by XRD methods.

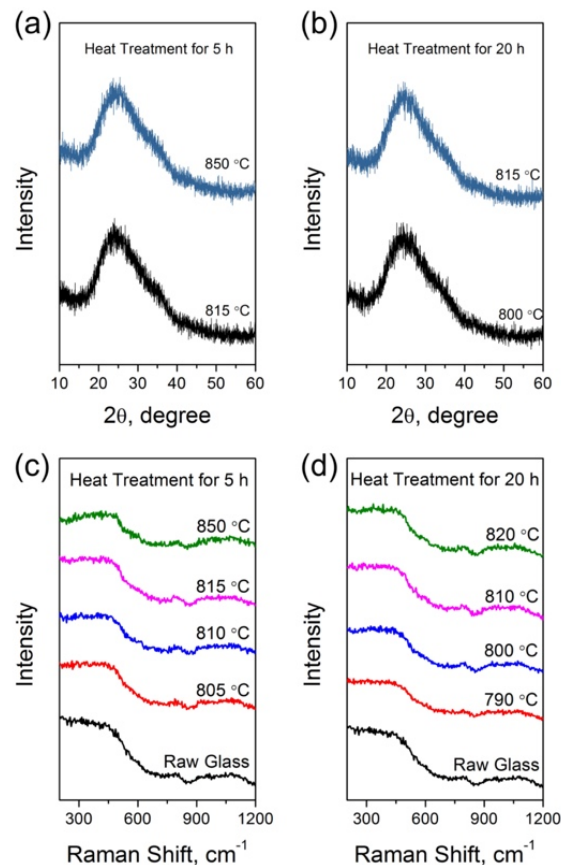


Figure 3. XRD patterns of glasses heat-treated for 5 h (a) and 20 h (b); Raman spectra of raw glass and glasses heat-treated for 5 h (c) and 20 h (d). Heat treatment temperatures are indicated.

The Raman spectra (Figure 3c,d) also demonstrate that there are no changes resulting from the heat treatment of the glasses, indicating the absence of bulk crystallization in the studied samples.

To study the microstructure of the glasses in detail, we analyzed images obtained by high-resolution TEM (HRTEM), which allowed us to distinguish the visualization of phase and chemical contrast that is not possible by other methods [26]. Figure 4 shows TEM images for samples 815-5 and 850-5. For sample 815-5, one can clearly observe the presence of zones on the order of 10–15 nm in size that stand out significantly in chemical contrast but on closer inspection have no discernible crystal planes. Such regions were previously described in glasses of the ZnO-Al₂O₃-SiO₂ system and attributed to regions of amorphous phase separation, wherein the glass matrix is enriched in SiO₂ and the amorphous phase inhomogeneities are enriched in ZnO [27]. The analysis of HRTEM images of sample 810-5 demonstrates that NPs of the order of 5 nm in size are formed within and between the amorphized regions; a detailed analysis of the interplanar distances in the NPs shows values of 0.23 and 0.2 nm, which correspond to the (111) and (200) planes in the Au crystal lattice. It should be noted that a similar pattern was obtained for sample 800-5. At the same time, for the sample 850-5, amorphous regions are not detected; moreover, even on the large scales, crystalline particles immediately become visible, which on closer examination were then identified by us to be gold NPs (Figure 4b).

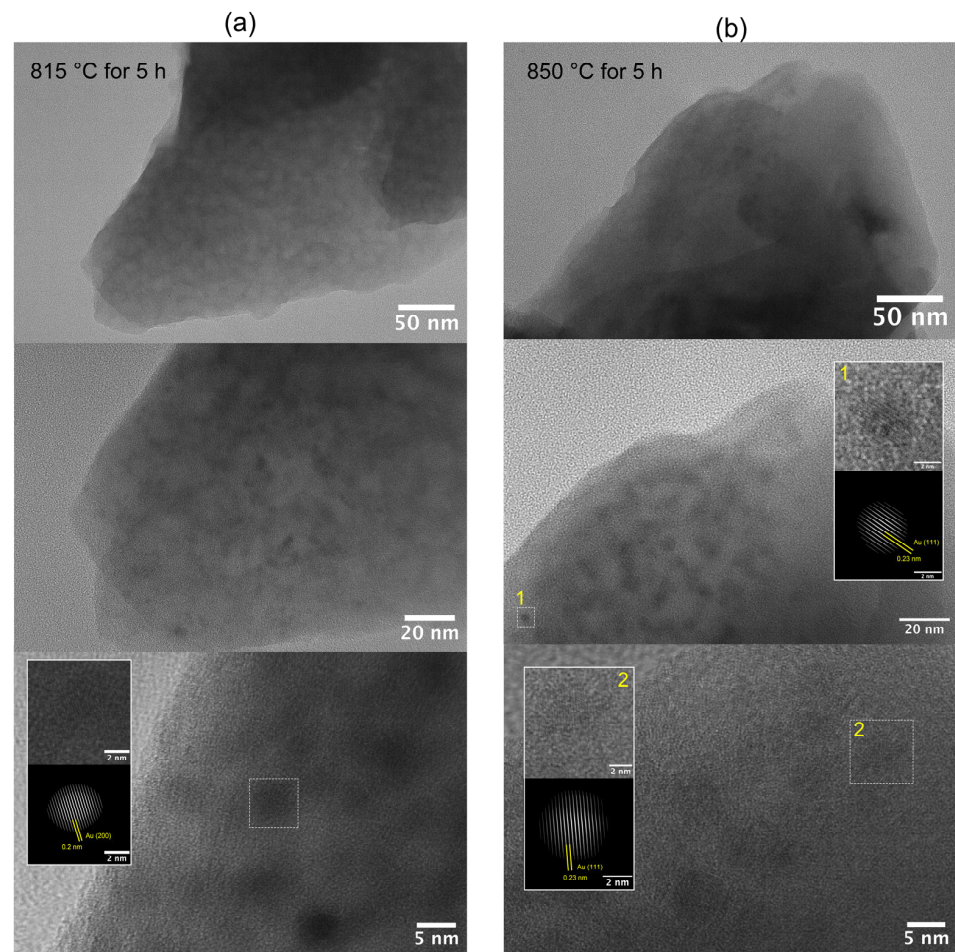


Figure 4. TEM and HRTEM images of glass samples heat-treated for 5 h at 815 °C (a) and 850 °C (b). Insets show enlarged images and Fourier-filtered images of the marked zones with corresponding numbers.

Figure 5a–c show the size distributions of NPs obtained by analyzing images of glass samples heat-treated for 5 h. It can be seen that when the treatment temperature is increased from 800 to 815 °C, the size of NPs does not change much and is approximately equal to 5 nm. At the same time, growth of the treatment temperature up to 850 °C leads to an increase in the size of NPs up to 6 nm on average. The analysis of TEM images (Figure 4) also demonstrates a more clustering tendency of nanoparticles rather than a uniform distribution in the glass matrix. In this regard, we analyzed the distance between the particles for each of the samples (Figure 5d–f). It can be seen that for the samples 800-5 and 815-5, the particle spacing is on average within 6 nm, while for the sample 850-5, the spacing increases and is on average within 8–10 nm. Such changes in the particle size and spacing for sample 850-5 compared with samples 800-5 and 815-5 are in some agreement with changes in the shape of the LSPR band in the absorption spectra of these samples. To study these relationships in more detail, we also studied the microstructure of samples heat-treated for 20 h.

Figure 6 shows TEM images for sample 800-20. As in the previous case, the images show clearly visible areas of amorphous phase separation, the sizes of which can be estimated within 15 nm on average. Analysis of the HRTEM images demonstrates the presence of gold NPs in the microstructure, which is confirmed by the size of interplanar distances in crystalline microdomains corresponding to the (111) and (200) planes in the Au crystal lattice. The distribution of NPs is also characterized by their clustering, but the analysis of the images does not allow us to draw an unambiguous conclusion as to whether this occurs between the phase separation regions or within them.

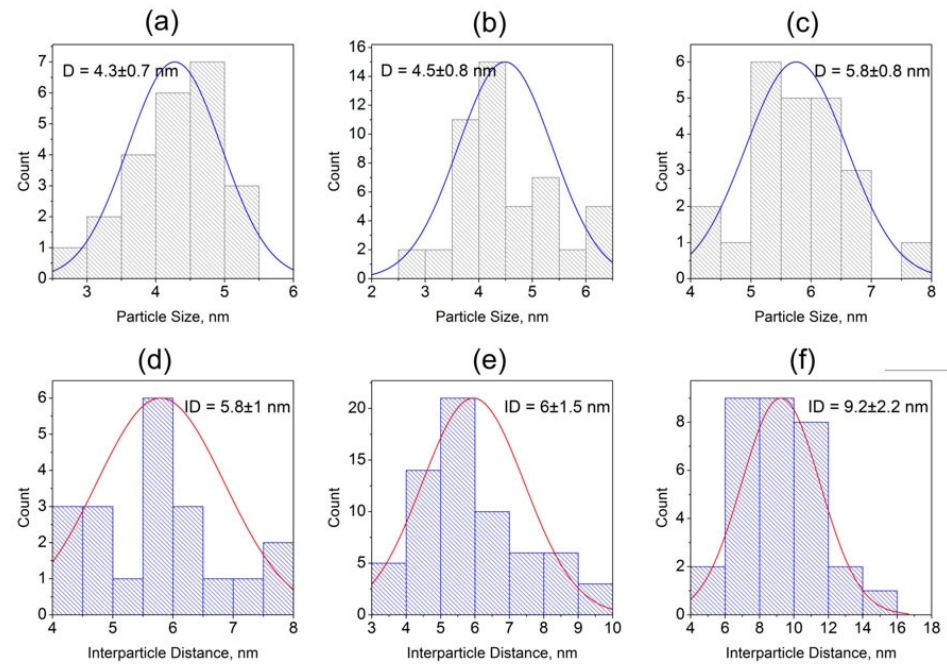


Figure 5. Particle size distribution (a–c) and interparticle distance (d–f) obtained from the TEM images of the glass samples treated for 5 h at 800, 815, and 850 °C (from left to right).

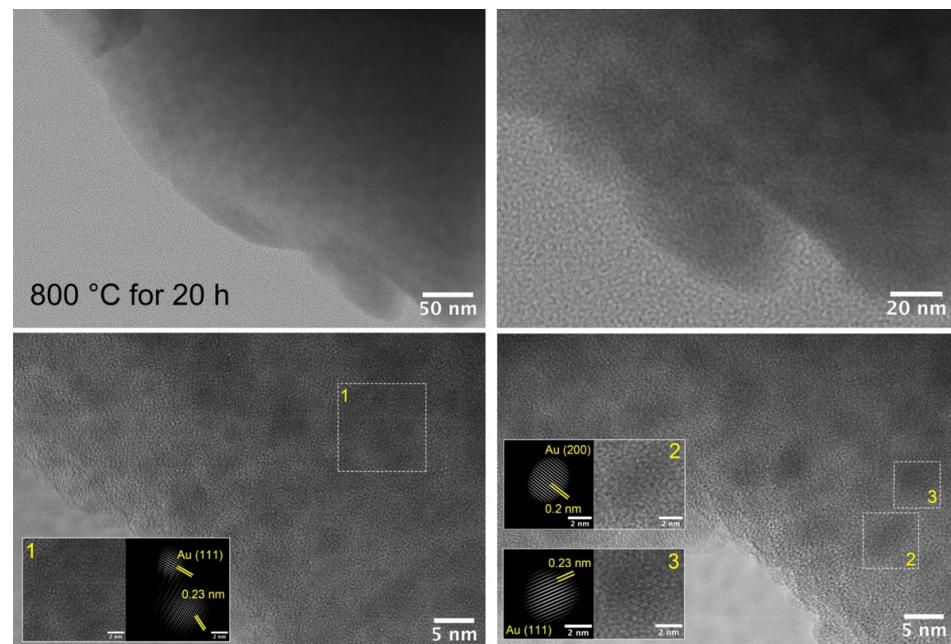


Figure 6. TEM and HRTEM images of glass samples heat-treated for 20 h at 800 °C. Insets show enlarged images and Fourier-filtered images of the marked zones with corresponding numbers.

A similar situation is observed for the sample 810-20 (Figure 7). TEM images show that the glass microstructure is characterized by an amorphous phase separation, with microdomain sizes on the order of 15 nm. Image analysis demonstrates that most of the NPs are located inside the liquation zones, which are presumably enriched with ZnO.

For the glass sample 815-20, TEM images show several striking differences in the microstructure (Figure 8). First, the images lack the pronounced zones of phase inhomogeneity that are evident in the images of samples 800-20 and 810-20. Secondly, the analysis of interplanar distances in crystal particles shows that along with gold NPs, crystals of another nature are formed in the glass; the values of the interplanar distances in them

are in the range of 0.27–0.3 nm. The exact determination of the nature of these crystals is possible with the use of methods of higher resolution microscopy and local chemical analysis on the scale of units of nanometers, which is beyond the capabilities of this study. At the same time, it can be assumed that the observed crystalline inclusions may belong to the ZAS-s.s. phase, which according to [20] is formed in glasses of this composition at close treatment temperatures.

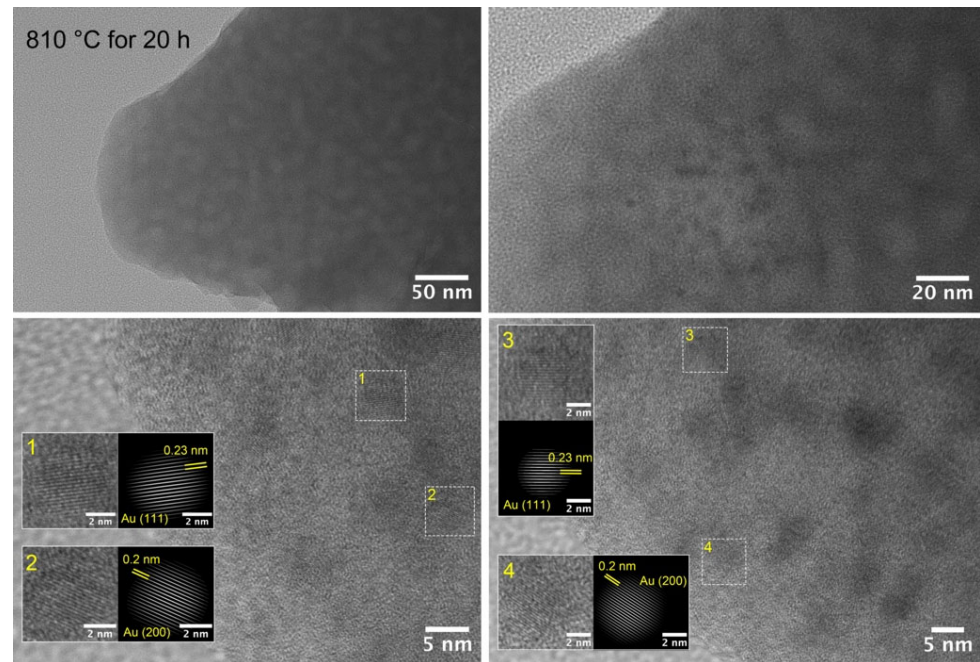


Figure 7. TEM and HRTEM images of glass samples heat-treated for 20 h at 810 °C. Insets show enlarged images and Fourier-filtered images of the marked zones with corresponding numbers.

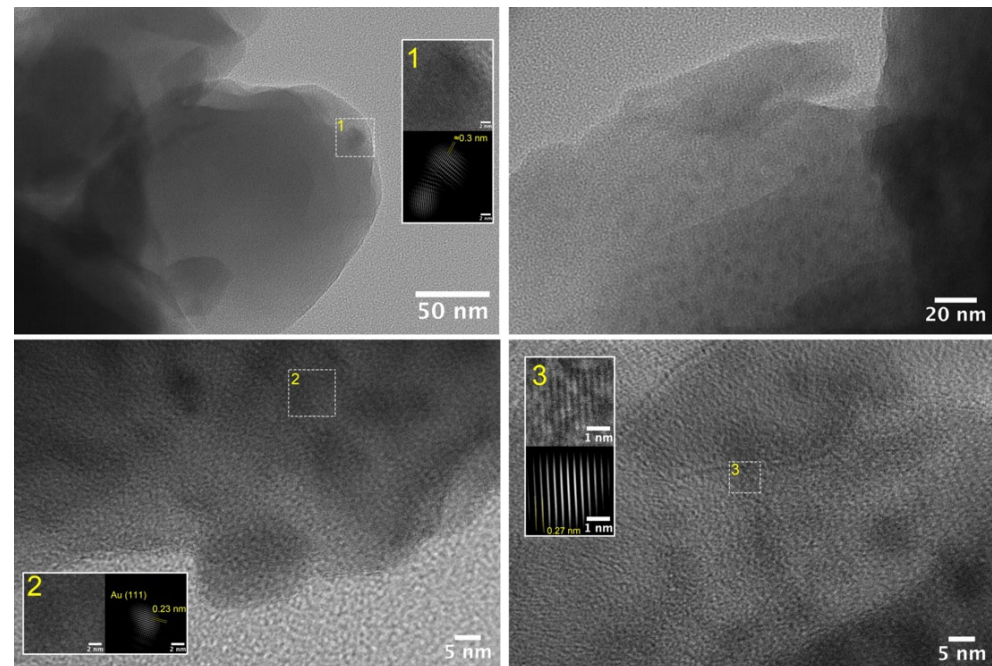


Figure 8. TEM and HRTEM images of glass samples heat-treated for 20 h at 815 °C. Insets show enlarged images and Fourier-filtered images of the marked zones with corresponding numbers.

Figure 9a–c shows the NP size distributions for glasses heat-treated for 20 h. It can be seen that with increasing treatment temperature, the average particle size increases from ≈ 4 nm to ≈ 7 nm. At the same time, the average distance between particles also increases from ≈ 5 nm at 800 °C to ≈ 11 nm when treated at 815 °C (Figure 9d–f).

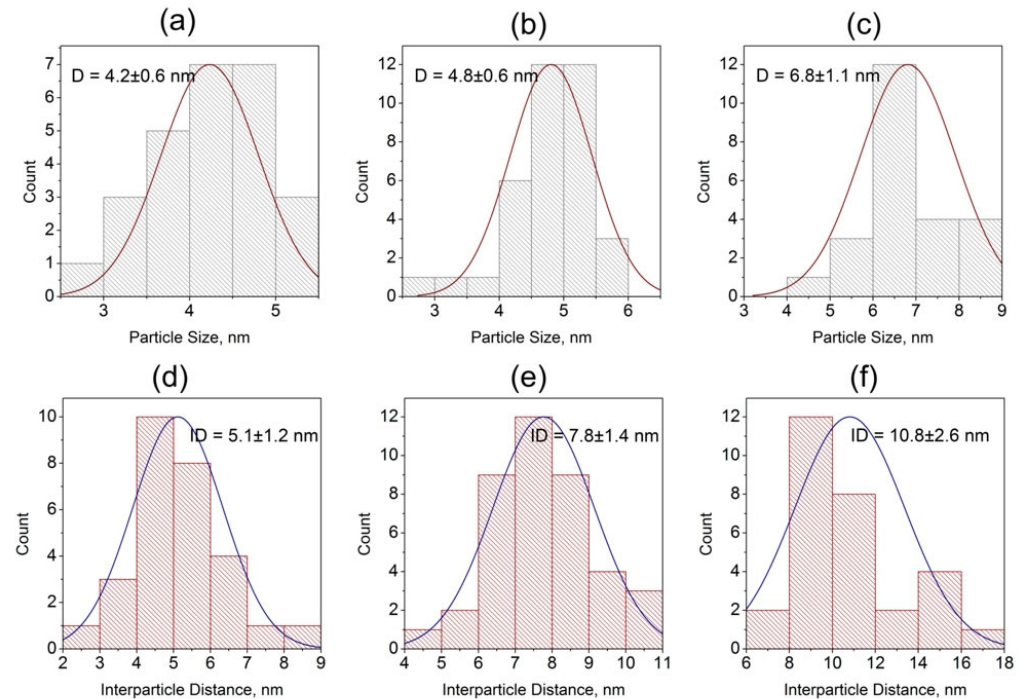


Figure 9. Particle size distribution (a–c) and interparticle distance (d–f) obtained from the TEM images of the glass samples treated for 20 h at 800, 810, and 815 °C (from left to right).

4. Discussion

The analysis of the obtained results allows us to conclude that in this work, during the heat treatment of ZAS glass containing Au additives, it was possible to form gold NPs, which have an ultra-wide LSPR band (over 1000 nm); meanwhile, changing the parameters of heat treatment allowed us to vary the shape and position of the band. In our opinion, these results are of interest both from the fundamental scientific point of view and in terms of finding certain practical applications. However, it is also important to determine the mechanism responsible for such a change in optical properties.

The factors that influence the change in the shape and position of the LSPR band of metal NPs (Au, Ag, Cu) in glasses include: (i) change in the size of nanoparticles; (ii) change in the shape of nanoparticles; (iii) change in the refractive index of the medium around the nanoparticle; and (iv) the presence of interactions between closely spaced nanoparticles. Each of these factors is further discussed in detail below.

(i) It is known that an increase in the size of NPs in glass leads to a change in the color of the glass caused by an increase in the intensity and change in the shape of the LSPR band, as well as a shift of the band maximum to the red region of the spectrum [11,28]. Thus, in many works using different glass-forming systems, it has been shown that by increasing the temperature of glass treatment, there is a process of increasing the size of NPs; the associated first increase is in the intensity, and then the red shift of the LSPR band occurs [28–30]. In [14], it was shown that increasing the size of gold NPs formed in tellurite glass leads to both broadening of the LSPR band and the manifestation of a dichroism effect similar in description to that obtained in our work. At the same time, in our work, despite the fact that the TEM data (Figures 5 and 9) show an increase in the size of gold NPs with an increasing treatment temperature, the dynamics of the change in the position and shape of the LSPR bands do not correspond to the previously described results. Moreover,

the results of the calculations of the LSPR band of gold NPs in ZAS glass medium does not describe the experimental spectra in any way. Figure 10 shows that in spite of the nanoparticle size, the calculated spectra are far away from the experimental results. Thus, only the change in the size of gold NPs in the process of the heat treatment does not allow us to describe the mechanism of the ultra-broadening of the LSPR band.

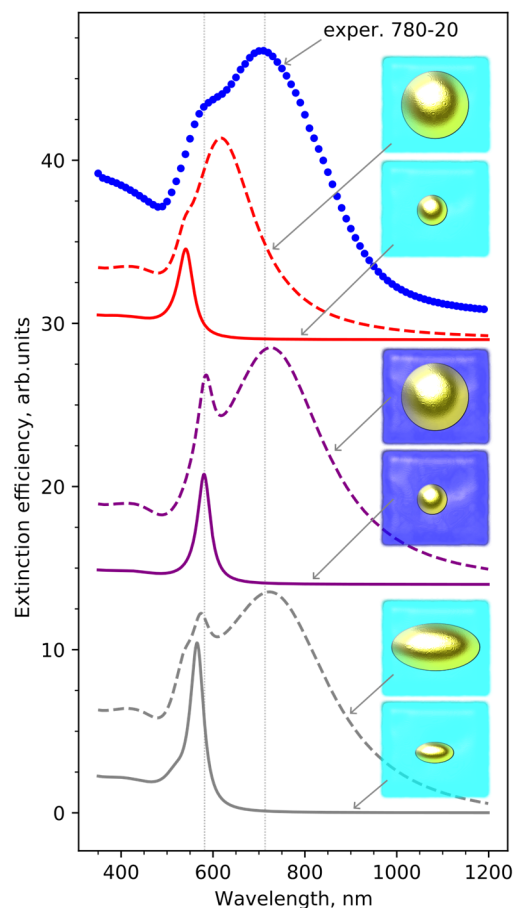


Figure 10. The comparison of the experimental absorption spectrum of the sample 780-20 (blue dots) with the calculated spectra for different models of single gold NPs: top panel—50 nm spherical particle (red dashes) and 10 nm spherical particle (solid red), both in the in matrix with $n_D = 1.6$; middle panel—50 nm spherical particle (purple dashed) and 10 nm spherical particle (solid purple), both in the in matrix with $n_D = 2.0$; bottom panel—60 nm oblate spheroid particle and 10 nm oblate spheroid particle, both in the in matrix with $n_D = 1.6$. The smaller 10 nm particles cannot explain the experimental data, while big particles (50–60 nm) are able to describe the experiment but are not presented in the sample.

(ii) Changing the shape of NPs to a shape other than spherical has a significant effect on the LSPR band and the position of the LSPR maximum: elongated particles are characterized by the splitting of the LSPR band into two components (with two maxima: one each in the short-wave and long-wave regions of the spectrum), which become dependent on the polarization of the incident light [31,32]. The formation of elongated NPs in glasses has been demonstrated using a variety of systems and methods, including mechanical deformation of glasses where spherical NPs are formed [33–35] and as a result of intensive laser irradiation of glasses with NPs [36,37]. In a series of papers by Som T. and Karmakar B., Sb_2O_3 -based glasses with elliptical gold NPs with aspect ratios ranging from 1.2 to 2.1 were synthesized. The glasses exhibited a dichroism effect similar to that described in our work, where the LSPR band for compositions with high Au content in the cited works was broadened, the band maximum shifted to the red region, and no splitting of

the band into two components was observed. The authors attributed the mechanism of deformation of gold NPs to the high viscosity of the glass melt without providing additional explanations; the authors also did not provide the calculated spectra of the LSPR bands for the experimentally determined sizes of NPs, so it is not possible to validate the proposed model [25,38]. An analysis of the TEM images in our work demonstrates that the shape of most NPs is close to spherical and the presence of elongated or elliptical particles could not be detected. Fitting of the experimental spectrum of the sample 780-20 with elliptical particles (Figure 10 bottom panel) allows us to describe the spectrum, but the size of NPs corresponding to the calculated spectrum should be larger than 58 nm with an aspect ratio of 1.63, which is not confirmed by the TEM data or by the data of the XRD and Raman spectroscopy; the presence of such large particles should be detected in X-ray diffraction patterns and Raman spectra, which was not observed experimentally (Figure 3).

(iii) The refractive index of the medium around NPs has a great influence on the position of the LSPR band. As the refractive index increases, the maximum of the band shifts to the red region of the spectrum; this effect is the basis for sensors that can detect trace amounts of chemical substances [39]. Using this effect, noble-metal NPs were synthesized in amorphous films based on SiO₂ containing different contents of oxides with high refractive indexes (TiO₂, ZrO₂). At the same time, the position of the LSPR band maximum in these NPs was tuned in the range of up to 600 nm by varying the content of the oxides with high refractive indexes, thus changing the average value of the refractive index of the medium around NPs [40,41]. Moreover, based on this effect, in our previous works [42,43], we have shown the possibility for tuning the position of the maximum of the LSPR band of gold NPs in glasses of the ZnO-MgO-Al₂O₃-SiO₂ system containing TiO₂ and ZrO₂ additives. During heat treatment in glasses along with the growth of NPs, the processes of phase separation first took place with the formation of amorphized zones enriched in TiO₂ and ZrO₂ (components with high refractive index); with the further increase in the temperature of the treatment, ZnAl₂O₄ crystals were formed in glasses, while TiO₂ and ZrO₂ components were uniformly distributed in the matrix. Amorphized zones enriched in TiO₂ and ZrO₂ increased the local refractive index of the medium around NPs, which influenced the position of the LSPR band, the maximum of which was shifted by more than 100 nm to the red region of the spectrum.

The analysis of TEM images in the current work also demonstrates the presence of phase separation zones (Figures 6 and 7), but due to the fact that the glass composition does not contain TiO₂ and ZrO₂, the chemical composition of the liquation zones seems to be enriched only in ZnO [27]. The refractive index n_D for ZnO is in the range of 1.6–1.78 according to the research data [44,45], which is not very different from the refractive index value for glass ($n_D = 1.569$); however, at the same time, it may have an effect on the LSPR band shift. The variation of the refraction index in the simulated optical spectra lead to a very high values, such as above 2.0 (Figure 10 middle panel). Such high refraction index values are not expected in the glass under the study as the densest component, ZnO, has a refraction index that is not higher than 2.0, but this phenomenon may have a partial effect on the overall LSPR band's position and shape.

(iv) The interaction between closely spaced plasmonic NPs can also be considered as a factor that has a great influence on the optical properties of the whole system [46]. It was experimentally demonstrated that a systematic change in the distance between gold NPs on the SiO₂ surface from 15 to 0.5 nm leads to a nonlinear broadening of the LSPR band. At a minimum distance, the dipole–dipole interaction between gold NPs leads to a maximum broadening of the band [47], and the authors showed that such a system is well described within the Maxwell–Garnett theory. In another work, gold NPs formed by a femtosecond laser beam on the Al₂O₃ substrate showed a broadened LSPR band at the highest irradiation energies, which was also explained by the reduction of the distance between NPs and their intense dipole–dipole interaction [48]. Jiménez J.A. et al., in a series of works with phosphate glasses containing NPs of silver, gold, and copper, also described the effect of the nonlinear broadening of the LSPR band in the framework of the

dipole and plasmonic interaction of closely spaced NPs [22,23,49]. For these glasses, the authors also described a dichroism effect similar to the effect obtained in the glasses in this work. Laser irradiation of the initial glass with NPs acted as a driver for the formation of zones with increased content of closely located silver NPs, which led to the formation of “super-nucleation” domains separated by amorphous zones of 15–20 nm in size, not containing NPs [49].

A comparative analysis of the change in the position of the LSPR band of the studied glass samples heat-treated for 20 h, as well as their calculated sizes and distances between the particles depending on the treatment temperature, is shown in Figure 11. It can be seen that the shift of the maximum of the LSPR band from ≈ 1100 nm to ≈ 600 nm with increasing treatment temperature is accompanied by an increase in both NPs sizes and distances between them. This suggests that the effect of the ultra-broadening of the LSPR band in glasses observed in this work can be related to the plasmonic interaction between closely spaced NPs.

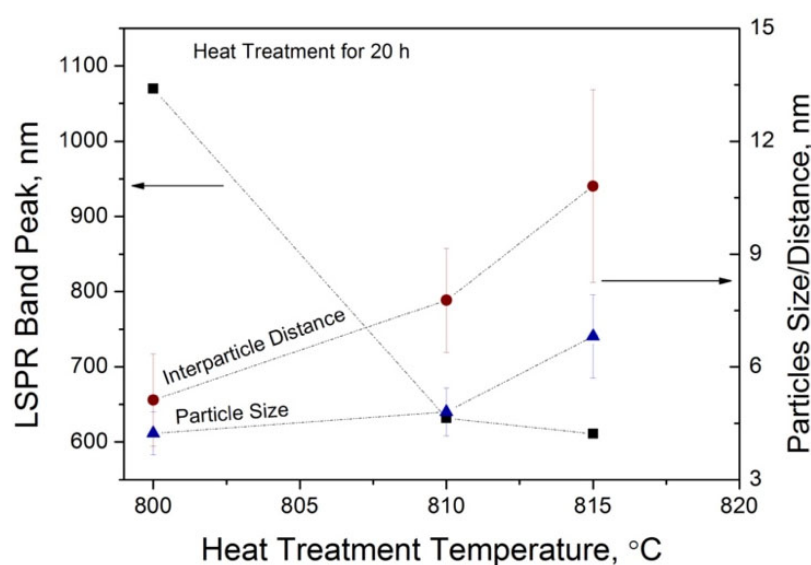


Figure 11. Evolution with heat treatment temperature at 20 h for the following parameters: LSPR band peak position (squares), particle size (triangles), and interparticle distance (circles).

To verify this hypothesis, we calculated the optical absorption spectra for agglomerates of NPs using a multiple spheres T-matrix approach, as implemented in MSTM code [50,51]. In the calculations, the NPs were represented as spheres with dielectric function as calculated by the Riuox formula [52] in a medium with a refractive index of 1.6. To simulate the closely packed agglomerate, the centers of the spheres were located at the nodes of a face-centered lattice with spacing so that the gap between NPs was 1 nm. The size of NPs of 10 nm and gap between them of 1 nm were selected as the smallest possible value for which the classical electrodynamic calculations are valid. The consideration of smaller sizes requires an application of size-corrected dielectric functions, and smaller gaps lead to the rise of electron tunneling.

Figure 12a shows the results of the calculations of the absorption spectra of an isolated gold nanoparticle of 10 nm and agglomerates of NPs of the same size containing 19, 43, and 87 NPs. It can be seen that as the number of particles in the agglomerate increases from 1 to 87, there is a shift in the main absorption maximum. However, the magnitude of this shift is on the order of 50 nm, which does not allow us to describe the observed shifts in resonance from 600 to 750 nm or more. However, in addition to the shift in the position of the main peak, a tendency to decrease its intensity and increase the intensity of the satellite long-wavelength peak as the number of NPs in the agglomerate increases is noticeable. In case of the agglomerate of 87 NPs, the intensities of these peaks are equalized. The trend is such that as the number of NPs in the agglomerate increases, one would

expect to reproduce the experimental curve. However, the quantitative description requires computation resources that are too extensive. Nevertheless, based on the obtained data, we assume that the agglomeration of NPs may be the main contributor to the visible splitting of the LSPR bands and their significant broadening.

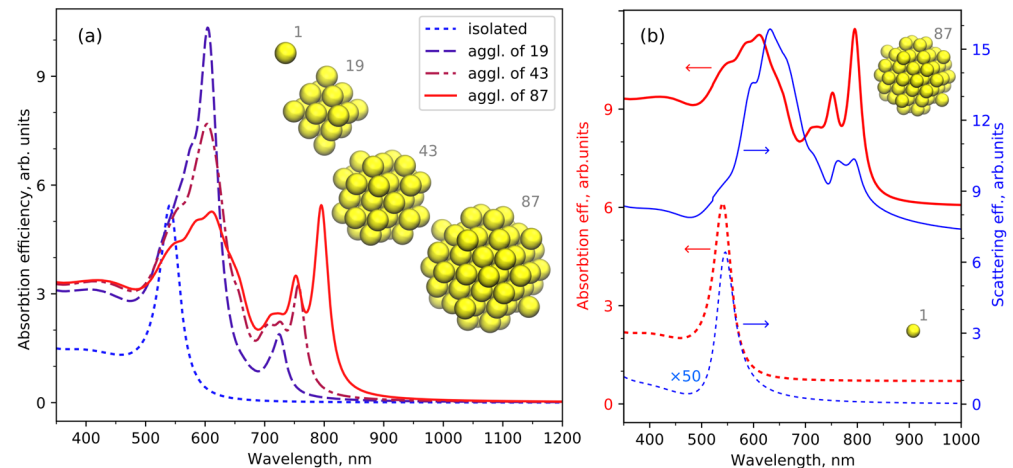


Figure 12. (a) The absorption efficiencies calculated for isolated gold nanoparticle and agglomerates containing 19, 43, or 87 nanoparticles. (b) The absorption (left y axis) and scattering (right y axis) efficiencies calculated for an agglomerate of 87 nanoparticles (solid curves) and isolated nanoparticles (short dashes).

Figure 12b compares the absorption and scattering spectra calculated for the isolated nanoparticle and the agglomerate of 87 NPs. The wavelength position of the absorption and scattering peaks are almost identical so that there is no difference in the transmitted and reflected color of the sample. In contrast, the scattering and absorption spectra for agglomerates are very different, which alter the color of material depending on the sample illumination. The experimental reflectance spectra of the studied glasses (Figure S2) are in line with the theoretical one showing intense reflection in the 650–750 nm range. This explains the observed dichroism of the samples by the presence of closely packed agglomerates of NPs.

Thus, the scenario of the changes in the optical properties of glasses observed in this work can be explained as follows. Phase separation processes take place in the glass during the heat treatment in a narrow temperature range. As a result, the formation of the localized amorphous regions on the order of 15 nm in size, apparently enriched in ZnO, occurs. In these regions, the formation of NPs can be energetically more favorable, so it leads to the formation of a kind of “plasmonic domains” with a high concentration of closely located particles, which is expressed in their plasmonic interaction and broadening of the LSPR spectrum. The presence of high concentrations of ZnO inside the domains can also lead to an increase in the local refractive index around the NPs and an additional redshift of the band. As the treatment temperature increases, the phase separation process is gradually replaced by the process of nucleation and growth of the crystalline phase, which is disintegrating the “plasmonic domains” and the distance between the nanoparticles increasing, which leads to a decrease in the plasmonic interaction effect and is expressed in the narrowing and blue shift of the LSPR band. At the same time, the increasing dichroism effect in the glass samples obtained by the heat treatment at higher temperature seems to also be related to the interactions between nanoparticles as well as formed nanocrystals of the ZAS-s.s. phase.

5. Conclusions

In conclusion, in this work, we have shown for the first time that it is possible to form gold NPs with an ultra-broad plasmon resonance (more than 1000 nm) in ZnO-Al₂O₃-SiO₂

glass. Precise thermal treatments of the glass allow for the tuning of the position and range of the LSPR band. The optical absorption spectroscopy results demonstrate that the LSPR band's position and shape can be finely controlled by varying the temperature during the treatment. The combination of Raman spectroscopy and XRD analysis reveals that the glasses remain completely amorphous despite prolonged treatment at temperatures above T_g . However, HRTEM results indicate that gold NPs with a size of approximately 5 nm are formed in the glass samples, along with amorphous areas of phase separation with sizes of around 15 nm. The mechanism responsible for the ultra-broadening of the LSPR spectrum and its redshift is attributed to the interparticle plasmonic coupling effect that is due to the formation of agglomerates containing a tenth of NPs with small distance between them, caused by the phase separation zones, which hinder the thermodiffusion of NPs. The presence of nanoparticle agglomerates is responsible for the observed dichroism. At higher treatment temperatures, the crystal nucleus (presumably ZAS-s.s.) forms in the sites of the amorphous phase separation zones, increasing the distance between NPs and significantly narrowing and shifting the LSPR band towards the blue region. The formation of gold NPs with an ultra-broad LSPR band in glasses holds promise for enhancing the luminescence of rare earth ions and advancing the development of novel photonic devices.

Supplementary Materials: The following supporting information can be downloaded at: <https://www.mdpi.com/article/10.3390/ceramics7020037/s1>, Figure S1: DSC curve of the synthesized glass; Figure S2: Reflectance spectra of the glass samples heat-treated for 20 h at temperatures in the 795–805 °C range.

Author Contributions: Conceptualization, G.S. and L.A.; methodology, G.A.; software, L.A.; validation, L.B., V.S. and M.V.; investigation, G.A., M.V., E.I., A.Z., M.Z. and E.S.; writing—original draft preparation, G.S.; writing—review and editing, L.A., E.I. and L.B.; visualization, L.A.; supervision, V.S.; funding acquisition, G.S. All authors have read and agreed to the published version of the manuscript.

Funding: This study was funded by the Russian Science Foundation grant No. 22-73-00236.

Data Availability Statement: Data are available upon request.

Acknowledgments: We thank N.V. Golubev for the XRD measurements and O.S. Dymshits for the fruitful discussion.

Conflicts of Interest: The authors declare no conflicts of interest.

References

1. Amendola, V.; Pilot, R.; Frascioni, M.; Maragò, O.; Iati, M. Surface Plasmon Resonance in Gold Nanoparticles: A Review. *J. Phys. Condens. Matter* **2017**, *29*, 203002. [[CrossRef](#)] [[PubMed](#)]
2. Ferrari, E. Gold Nanoparticle-Based Plasmonic Biosensors. *Biosensors* **2023**, *13*, 411. [[CrossRef](#)] [[PubMed](#)]
3. Sarfraz, N.; Khan, I. Plasmonic Gold Nanoparticles (AuNPs): Properties, Synthesis and Their Advanced Energy, Environmental and Biomedical Applications. *Chem. Asian J.* **2021**, *16*, 720–742. [[CrossRef](#)] [[PubMed](#)]
4. Shafiq, A.R.; Abdul Aziz, A.; Mehrdel, B. Nanoparticle Optical Properties: Size Dependence of a Single Gold Spherical Nanoparticle. *J. Phys. Conf. Ser.* **2018**, *1083*, 012040. [[CrossRef](#)]
5. Núñez-Leyva, J.M.; Kolosovas-Machuca, E.S.; Sánchez, J.; Guevara, E.; Cuadrado, A.; Alda, J.; González, F.J. Computational and Experimental Analysis of Gold Nanorods in Terms of Their Morphology: Spectral Absorption and Local Field Enhancement. *Nanomaterials* **2021**, *11*, 1696. [[CrossRef](#)] [[PubMed](#)]
6. Djorović, A.; Oldenburg, S.J.; Grand, J.; Le Ru, E.C. Extinction-to-Absorption Ratio for Sensitive Determination of the Size and Dielectric Function of Gold Nanoparticles. *ACS Nano* **2020**, *14*, 17597–17605. [[CrossRef](#)] [[PubMed](#)]
7. Yu, H.; Peng, Y.; Yang, Y.; Li, Z.-Y. Plasmon-Enhanced Light–Matter Interactions and Applications. *NPJ Comput. Mater.* **2019**, *5*, 45. [[CrossRef](#)]
8. Srabionyan, V.V.; Vetchinnikov, M.P.; Rubanik, D.S.; Durymanov, V.A.; Viklenko, I.A.; Avakyan, L.A.; Zinina, E.M.; Shakhgildyan, G.Y.; Sigaev, V.N.; Bugaev, L.A. Local Electric Field Enhancement in the Vicinity of Aggregates of Ag, Au, Rb Containing Nanoparticles in Oxide Glasses. *J. Non Cryst. Solids* **2024**, *631*, 122927. [[CrossRef](#)]
9. Shakhgildyan, G.; Lipatiev, A.; Lotarev, S.; Fedotov, S.; Sigaev, V. Glass: Home of the Periodic Table. *Front. Chem.* **2020**, *8*, 384. [[CrossRef](#)] [[PubMed](#)]
10. Shakhgil'dyan, G.Y.; Ziyatdinova, M.Z.; Kovgar, V.V.; Lotarev, S.V.; Sigaev, V.N.; Prusova, I.V. Effect of Gold Nanoparticles on the Spectral Luminescence Properties of Eu^{3+} -Doped Phosphate Glass. *Glass Ceram.* **2019**, *76*, 121–125. [[CrossRef](#)]

11. Savinkov, V.I.; Shakhgil'Dyan, G.Y.; Paleari, A.; Sigaev, V.N. Synthesis of Optically Uniform Glasses Containing Gold Nanoparticles: Spectral and Nonlinear Optical Properties. *Glass Ceram.* **2013**, *70*, 143–148. [[CrossRef](#)]
12. Som, T.; Karmakar, B. Plasmon Tuning of Nano-Au in Dichroic Devitrified Antimony Glass Nanocomposites by Refractive Index Control. *Chem. Phys. Lett.* **2009**, *479*, 100–104. [[CrossRef](#)]
13. Chen, F.; Dai, S.; Xu, T.; Shen, X.; Lin, C.; Nie, Q.; Liu, C.; Heo, J. Surface-Plasmon Enhanced Ultrafast Third-Order Optical Nonlinearities in Ellipsoidal Gold Nanoparticles Embedded Bismuthate Glasses. *Chem. Phys. Lett.* **2011**, *514*, 79–82. [[CrossRef](#)]
14. Wei, Y.; Zhao, J.; Fuhrmann, S.; Sajzew, R.; Wondraczek, L.; Ebendorff-Heidepriem, H. Controlled Formation of Gold Nanoparticles with Tunable Plasmonic Properties in Tellurite Glass. *Light Sci. Appl.* **2023**, *12*, 293. [[CrossRef](#)] [[PubMed](#)]
15. Lipat'ev, A.S.; Shakhgil'dyan, G.Y.; Lipat'eva, T.O.; Lotarev, S.V.; Fedotov, S.S.; Vetchinnikov, M.P.; Ignat'eva, E.S.; Golubev, N.V.; Sigaev, V.N.; Kazanskii, P.G. Formation of Luminescent and Birefringent Microregions in Phosphate Glass Containing Silver. *Glass Ceram.* **2016**, *73*, 277–282. [[CrossRef](#)]
16. Srabionyan, V.V.; Heinz, M.; Kaptelinin, S.Y.; Avakyan, L.A.; Sukharina, G.B.; Skidanenko, A.V.; Pryadchenko, V.; Abdulvakhidov, K.G.; Mikheykin, A.; Durymanov, V.; et al. Effect of Thermal Post-Treatment on Surface Plasmon Resonance Characteristics of Gold Nanoparticles Formed in Glass by UV Laser Irradiation. *J. Alloys Compd.* **2019**, *803*, 354–363. [[CrossRef](#)]
17. Heinz, M.; Srabionyan, V.V.; Avakyan, L.A.; Bugaev, A.L.; Skidanenko, A.V.; Pryadchenko, V.V.; Ihlemann, J.; Meinertz, J.; Patzig, C.; Dubiel, M.; et al. Formation and Implantation of Gold Nanoparticles by ArF-Excimer Laser Irradiation of Gold-Coated Float Glass. *J. Alloys Compd.* **2018**, *736*, 152–162. [[CrossRef](#)]
18. Schneider, C.A.; Rasband, W.S.; Eliceiri, K.W. NIH Image to ImageJ: 25 Years of Image Analysis. *Nat. Methods* **2012**, *9*, 671–675. [[CrossRef](#)] [[PubMed](#)]
19. Martín-Yerga, D.; Yu, X.; Terekhina, I.; Henriksson, G.; Cornell, A. In Situ Catalyst Reactivation for Enhancing Alcohol Electro-Oxidation and Coupled Hydrogen Generation. *Chem. Commun.* **2020**, *56*, 4011–4014. [[CrossRef](#)]
20. Cormier, L.; Delbes, L.; Baptiste, B.; Montouillout, V. Vitrification, Crystallization Behavior and Structure of Zinc Aluminosilicate Glasses. *J. Non Cryst. Solids* **2021**, *555*, 120609. [[CrossRef](#)]
21. Shakhgildyan, G.Y.; Ziyatdinova, M.Z.; Vetchinnikov, M.P.; Lotarev, S.V.; Savinkov, V.I.; Presnyakova, N.N.; Lopatina, E.V.; Vilkovisky, G.A.; Sigaev, V.N. Thermally-Induced Precipitation of Gold Nanoparticles in Phosphate Glass: Effect on the Optical Properties of Er³⁺ Ions. *J. Non Cryst. Solids* **2020**, *550*, 120408. [[CrossRef](#)]
22. Jiménez, J.A. Photoluminescence of Sm³⁺ Ions in Au-Doped Plasmonic and Dichroic Phosphate Glass. *Eur. Phys. J. D* **2023**, *77*, 124. [[CrossRef](#)]
23. Jiménez, J.A. Dichroism in Plasmonic Cu Nanocomposite Glass: Selective Enhancement of the Orange-Red Emission from Sm³⁺. *Opt. Mater. X* **2019**, *1*, 100002. [[CrossRef](#)]
24. Singh, S.P.; Nath, M.; Karmakar, B. Quantum and Dielectric Confinements of Sub-10 Nm Gold in Dichroic Phosphate Glass Nanocomposites. *Mater. Chem. Phys.* **2014**, *146*, 198–203. [[CrossRef](#)]
25. Som, T.; Karmakar, B. Surface Plasmon Resonance and Enhanced Fluorescence Application of Single-Step Synthesized Elliptical Nano Gold-Embedded Antimony Glass Dichroic Nanocomposites. *Plasmonics* **2010**, *5*, 149–159. [[CrossRef](#)]
26. Montazerian, M.; Mancini, M.; Mauro, J.C. Advanced Tools for Unveiling Nucleation in Nanostructured Glass-Ceramics. *Crit. Rev. Solid State Mater. Sci.* **2023**, *48*, 411–439. [[CrossRef](#)]
27. Jiazhi, L.; Ying, S.; Guangling, H. An Investigation of Relationship between Phase Separation and Crystallization of ZnO-Al₂O₃-SiO₂ Glasses. *J. Phys. Colloq.* **1982**, *43*, C9-231–C9-234. [[CrossRef](#)]
28. Pellerin, N.; Blondeau, J.-P.; Noui, S.; Allix, M.; Ory, S.; Veron, O.; De Sousa Meneses, D.; Massiot, D. Control of Selective Silicate Glass Coloration by Gold Metallic Nanoparticles: Structural Investigation, Growth Mechanisms, and Plasmon Resonance Modelization. *Gold Bull.* **2013**, *46*, 243–255. [[CrossRef](#)]
29. Sigaev, V.N.; Savinkov, V.I.; Lotarev, S.V.; Shakhgildyan, G.Y.; Lorenzi, R.; Paleari, A. Spatially Selective Au Nanoparticle Growth in Laser-Quality Glass Controlled by UV-Induced Phosphate-Chain Cross-Linkage. *Nanotechnology* **2013**, *24*, 225302. [[CrossRef](#)] [[PubMed](#)]
30. Simo, A.; Polte, J.; Pfänder, N.; Vainio, U.; Emmerling, F.; Rademann, K. Formation Mechanism of Silver Nanoparticles Stabilized in Glassy Matrices. *J. Am. Chem. Soc.* **2012**, *134*, 18824–18833. [[CrossRef](#)] [[PubMed](#)]
31. Grand, J.; Adam, P.-M.; Grimault, A.-S.; Vial, A.; Lamy de la Chapelle, M.; Bijeon, J.-L.; Kostcheev, S.; Royer, P. Optical Extinction Spectroscopy of Oblate, Prolate and Ellipsoid Shaped Gold Nanoparticles: Experiments and Theory. *Plasmonics* **2006**, *1*, 135–140. [[CrossRef](#)]
32. Pérez-Juste, J.; Pastoriza-Santos, I.; Liz-Marzán, L.M.; Mulvaney, P. Gold Nanorods: Synthesis, Characterization and Applications. *Coord. Chem. Rev.* **2005**, *249*, 1870–1901. [[CrossRef](#)]
33. Berger, A. Prolate Silver Particles in Glass Surfaces. *J. Non Cryst. Solids.* **1993**, *163*, 185–194. [[CrossRef](#)]
34. Mennig, M.; Berg, K.-J. Determination of Size Shape and Concentration of Spheroidal Silver Colloids Embedded in Glass by VIS-Spectroscopy. *Mater. Sci. Eng. B* **1991**, *9*, 421–424. [[CrossRef](#)]
35. Suszynska, M.; Krajczyk, L.; Capelletti, R.; Baraldi, A.; Berg, K.J. Microstructure and Silver Nanoparticles in Ion-Exchanged and Deformed Soda-Lime Silicate Glasses. *J. Non Cryst. Solids* **2003**, *315*, 114–123. [[CrossRef](#)]
36. Stalmashonak, A.; Matyssek, C.; Kiriyenko, O.; Hergert, W.; Graener, H.; Seifert, G. Preparing Large-Aspect-Ratio Prolate Metal Nanoparticles in Glass by Simultaneous Femtosecond Multicolor Irradiation. *Opt. Lett.* **2010**, *35*, 1671. [[CrossRef](#)] [[PubMed](#)]

37. Shakhgildyan, G.Y.; Lipatiev, A.S.; Fedotov, S.S.; Vetchinnikov, M.P.; Lotarev, S.V.; Sigaev, V.N. Microstructure and Optical Properties of Tracks with Precipitated Silver Nanoparticles and Clusters Inscribed by the Laser Irradiation in Phosphate Glass. *Ceram. Int.* **2021**, *47*, 14320–14329. [[CrossRef](#)]
38. Som, T.; Karmakar, B. Enhanced Frequency Upconversion of Sm³⁺ Ions by Elliptical Au Nanoparticles in Dichroic Sm³⁺: Au-Antimony Glass Nanocomposites. *Spectrochim. Acta Part A Mol. Biomol. Spectrosc.* **2010**, *75*, 640–646. [[CrossRef](#)]
39. Mayer, K.M.; Hafner, J.H. Localized Surface Plasmon Resonance Sensors. *Chem. Rev.* **2011**, *111*, 3828–3857. [[CrossRef](#)]
40. De, S.; Medda, S.K.; De, G. Refractive Index Controlled Plasmon Tuning of Au Nanoparticles in SiO₂-ZrO₂ Film Matrices. *J. Nanosci. Nanotechnol.* **2008**, *8*, 3868–3876. [[CrossRef](#)] [[PubMed](#)]
41. De, G.; Medda, S.K.; De, S.; Pal, S. Metal Nanoparticle Doped Coloured Coatings on Glasses and Plastics through Tuning of Surface Plasmon Band Position. *Bull. Mater. Sci.* **2008**, *31*, 479–485. [[CrossRef](#)]
42. Shakhgildyan, G.; Durymanov, V.; Ziyatdinova, M.; Atroshchenko, G.; Golubev, N.; Trifonov, A.; Chereuta, O.; Avakyan, L.; Bugaev, L.; Sigaev, V. Effect of Gold Nanoparticles on the Crystallization and Optical Properties of Glass in ZnO-MgO-Al₂O₃-SiO₂ System. *Crystals* **2022**, *12*, 287. [[CrossRef](#)]
43. Shakhgildyan, G.; Avakyan, L.; Ziyatdinova, M.; Atroshchenko, G.; Presnyakova, N.; Vetchinnikov, M.; Lipatiev, A.; Bugaev, L.; Sigaev, V. Tuning the Plasmon Resonance of Gold Nanoparticles in Phase-Separated Glass via the Local Refractive Index Change. *J. Non Cryst. Solids* **2021**, *566*, 120893. [[CrossRef](#)]
44. Stelling, C.; Singh, C.R.; Karg, M.; König, T.A.F.; Thelakkat, M.; Retsch, M. Plasmonic Nanomeshes: Their Ambivalent Role as Transparent Electrodes in Organic Solar Cells. *Sci. Rep.* **2017**, *7*, 42530. [[CrossRef](#)] [[PubMed](#)]
45. Aguilar, O.; de Castro, S.; Godoy, M.P.F.; Rebelo Sousa Dias, M. Optoelectronic Characterization of Zn_{1-x}Cd_xO Thin Films as an Alternative to Photonic Crystals in Organic Solar Cells. *Opt. Mater. Express* **2019**, *9*, 3638. [[CrossRef](#)]
46. Ghosh, S.K.; Pal, T. Interparticle Coupling Effect on the Surface Plasmon Resonance of Gold Nanoparticles: From Theory to Applications. *Chem. Rev.* **2007**, *107*, 4797–4862. [[CrossRef](#)] [[PubMed](#)]
47. Ung, T.; Liz-Marzán, L.M.; Mulvaney, P. Optical Properties of Thin Films of Au@SiO₂ Particles. *J. Phys. Chem. B* **2001**, *105*, 3441–3452. [[CrossRef](#)]
48. Nedyalkov, N.N.; Nakajima, Y.; Takami, A.; Koleva, M.; Karashanova, D.; Terakawa, M. Laser Induced Morphological and Optical Properties Changes in Au Doped Aluminum Oxide and Silicon Oxide Thin Films. *Opt. Laser Technol.* **2016**, *79*, 179–187. [[CrossRef](#)]
49. Sendova, M.; Jiménez, J.A. Plasmonic Coupling in Silver Nanocomposite Glasses. *J. Phys. Chem. C* **2012**, *116*, 17764–17772. [[CrossRef](#)]
50. Mackowski, D.W.; Mishchenko, M.I. A Multiple Sphere T-Matrix Fortran Code for Use on Parallel Computer Clusters. *J. Quant. Spectrosc. Radiat. Transf.* **2011**, *112*, 2182–2192. [[CrossRef](#)]
51. Avakyan, L.A.; Heinz, M.; Skidanenko, A.V.; Yablunovskii, K.A.; Ihlemann, J.; Meinertz, J.; Patzig, C.; Dubiel, M.; Bugaev, L.A. Insight on Agglomerates of Gold Nanoparticles in Glass Based on Surface Plasmon Resonance Spectrum: Study by Multi-Spheres T-Matrix Method. *J. Phys. Condens. Matter* **2018**, *30*, 045901. [[CrossRef](#)] [[PubMed](#)]
52. Rioux, D.; Vallières, S.; Besner, S.; Muñoz, P.; Mazur, E.; Meunier, M. An Analytic Model for the Dielectric Function of Au, Ag, and Their Alloys. *Adv. Opt. Mater.* **2014**, *2*, 176–182. [[CrossRef](#)]

Disclaimer/Publisher’s Note: The statements, opinions and data contained in all publications are solely those of the individual author(s) and contributor(s) and not of MDPI and/or the editor(s). MDPI and/or the editor(s) disclaim responsibility for any injury to people or property resulting from any ideas, methods, instructions or products referred to in the content.